

Case Study: Design of Flood Control Systems on the Vara River by Numerical and Physical Modeling

Annunziato Siviglia¹; Alessandro Stocchino²; and Marco Colombini³

Abstract: In the present paper, we investigate the effectiveness of a flood defense project based on storage reservoirs, presently under study for the Magra River and Vara River (Italy). We have focused the analysis on two detention reservoirs and studied their response to different hydrological scenarios mostly in terms of flood mitigation efficiency, leaving aside sediment transport issues. The analysis has been carried out with the aid of a physical model and one-dimensional numerical simulations. Experimental and numerical simulations have been performed spanning a wide range of hydrological conditions. Some of the results can be generalized for different applications where similar flood control systems are employed.

DOI: 10.1061/(ASCE)HY.1943-7900.0000135

CE Database subject headings: Floods; Numerical models; Italy; Design; Case studies.

Introduction

Water management measures are closely linked to a variety of needs within human society. If on one hand, they have to improve the water utilization for different purposes. On the other hand, they must also provide a protection against the possible destructive effects, e.g., during a flood event.

Flood control projects are of crucial importance in preserving lands from the occurrence of natural disasters caused by river floods. A great variety of flood control measures are available that can be generally classified as structural projects, which rely on different kinds of hydraulic structures and nonstructural projects. Among the structural measures, detention reservoirs have proven to be effective in reducing downstream flooding risk. Reservoirs are designed to temporarily store floodwater behind dams or inside detention basins. In the present paper, we investigate the effectiveness of a flood mitigation project based on storage reservoirs to be built on the Vara River (Italy). The Vara River is the main tributary of the Magra River, which has a basin of about 1,698 km² and is confined between the basin of the Po River (North) and the Tyrrhenian Sea (South), crossing the Tuscany and Liguria regions. The Vara basin has a watershed of about 600 km², with average annual rainfall of about 1,770 mm/y and

an estimated average inflow of about 570×10^6 m³ per year. The purpose of river training is primarily to control floods with a particular attention being given to the protection of floodplains and human settlements (Wu et al. 2005). Starting from the identification of vulnerable regions in the basin, the actions considered in the mentioned plan are mainly aimed to regulate the floodwater and to control the sediment conveyance along the entire river. The feasibility of a system of relatively small volume floodwater reservoirs distributed on the entire basin, taking advantage of the limited natural floodplains, has been studied. The number of the reservoirs distributed on the entire network should be 29 for an available total volume of about 20×10^6 m³, for a corresponding cost estimated to be about 110 million euros.

Many examples of distributed flood control-systems are reported in the literature, see for instance Avakyan and Polyushkin (1989), Slutzman and Smith (2006), and Giesecke (2007). In the present work, we have studied in detail a system of two floodwater storage reservoirs located in the upper part of the Vara River. In particular, we

- Evaluate the flood mitigation effects produced by the flood control measures;
- Compare the performance of different configurations of the flood control systems;
- Investigate the response of a system of multiple detention basins to different hypothetical floods with a wide range of occurrence periods, eventually suggesting a simple relationship to estimate the global flood attenuation efficiency;
- Produce a rating curve appropriate to describe the hydraulic behavior of the designed dam, which might be generalized to other dams of the same kind but with different geometrical characteristics; and
- Formulate a 1D numerical model capable to describe the unsteady dynamics of the flood propagation and attenuation produced by the presence of the detention basins.

To accomplish the above tasks, we make use of both numerical and a physical modeling specifically designed in order to reproduce one of the two floodwater control structures.

¹Dr., Dept. of Civil and Environmental Engineering, Univ. of Trento, via Mesiano 77, Trento 38050, Italy (corresponding author). E-mail: nunzio.siviglia@ing.unitn.it.

²Dr., Dept. of Civil, Environmental, and Architectural Engineering, Univ. of Genova, via Montallegro 1, Genova 16145, Italy. E-mail: jorma@dicat.unige.it

³Professor, Dept. of Civil, Environmental, and Architectural Engineering, Univ. of Genova, via Montallegro 1, Genova 16145, Italy. E-mail: marco.colombini@dicat.unige.it

Note. This manuscript was submitted on February 15, 2008; approved on July 8, 2009; published online on July 13, 2009. Discussion period open until May 1, 2010; separate discussions must be submitted for individual papers. This paper is part of the *Journal of Hydraulic Engineering*, Vol. 135, No. 12, December 1, 2009. ©ASCE, ISSN 0733-9429/2009/12-1063-1072/\$25.00.

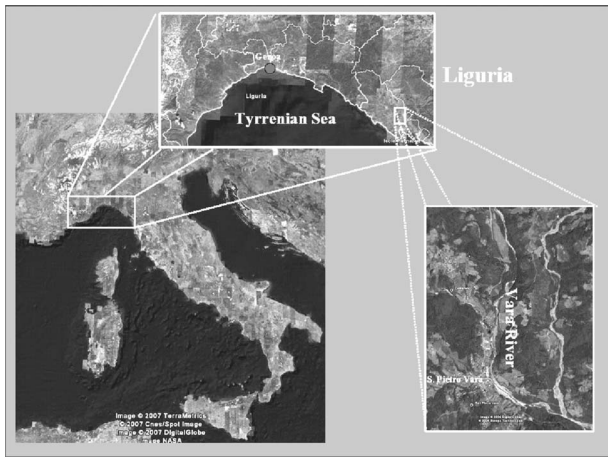


Fig. 1. Aerial photograph of the study area and its location

Study Area and Impounding Structures

The river reach under consideration extends for about 7 km in the Apennines region of its basin, close to a small village (S. Pietro Vara), see Fig. 1. The river reach is mainly single threaded and no important embankments or other river training structures (bend and bank protections) are present. Along this reach, two locations have been identified as possible sites for floodwater storage. The first, herein labeled VARA1, is placed upstream of the village, extending for 1 km with an available storage volume of about $3.7 \times 10^5 \text{ m}^3$. The second, herein labeled VARA2, is located just downstream S. Pietro Vara, is characterized by a greater available volume, i.e., $7 \times 10^5 \text{ m}^3$. An aerial image of the river reach is shown in Fig. 2, with the location of the detention reservoirs depicted in white. Between the two systems, four minor and three major tributaries are present and their contribution to the main channel discharge has been taken into account for the numerical simulations.

In the present study, two different configurations of the flood defense systems are considered: the first configuration, denoted as “L1,” consists of a rock-earth-fill dam with a bottom gate and a top spillway; the second configuration, denoted as “M1,” consists of the same dam together with a longitudinal embankment, which has a lateral spillway near the dam (see Fig. 3). A sketch of the main geometrical characteristics of the transverse and lateral structures is shown in Fig. 4 and the geometrical characteristics of the dams are given in Table 1.

The main design parameters considered can be summarized as follows: (1) a design discharge Q_D , which is related to a certain return period T_R that depends on the hydrologic characteristics of the basin, in the present case $T_R=30$ years; (2) the maximum acceptable free surface elevation in the case of occurrence of an extreme event in the present case $T_R=200$ years—which is necessarily related to the available volume; (3) the minimum discharge for which the system starts to interact significantly with the flow. The main output of the preliminary design will be the determination of the flood attenuation defined as

$$\varepsilon = \frac{Q_{IN} - Q_{OUT}}{Q_{IN}} \quad (1)$$

where Q_{IN} =peak of the entering hydrograph and Q_{OUT} =maximum discharge that flows through the dam. In other words, it indicates the amount of reduction of the peak of the incoming hydrograph. A correct rating curve describing the hydraulic re-



Fig. 2. Aerial photograph of the river reach under study. The boundary of the two detention reservoirs are sketched in white.

sponse of the transverse structure is necessary in order to accomplish the preliminary design described above. For this reason in the present study the determination of the rating curve of the dam was the first step of our experiments.

Detailed data have been collected at the beginning of the study. In particular, a topographic survey was carried out in the region of interest. Moreover, during a field trip along the river reach, armor samples were collected in order to estimate the surface roughness (Parker 1990), employing the statistical sampling called pebble counts (Bunte and Abt 2001).

Finally, hydrographs for different return periods, ranging from 5 to 200 years, were provided by the Authority for the river reach entering the VARA1 reservoir. The corresponding peak discharges range from 159 to 815 m^3/s .

Physical Model and Measurements

The present physical model has been designed preserving the Froude number of the prototype, imposing a geometrical scale of 1:62.5. The river reach under investigation is about 1-km-long and the area of the river-basin [bounded by the contour line corresponding to a value of 325 m above mean sea level (AMSL)] is about 0.2 km^2 . Therefore, the physical model is about 16-m-long and 6-m-wide. A schematic representation of the model is shown in Fig. 3. In the same figure, the contour lines representing the orography and the floodplain are clearly visible, whereas in the main channel the cross sections are reported as straight lines.

Using similitude based on the Froude number implies that the resistance in the model follows a prescribed scale. In particular, the dimensional analysis suggests that the coefficient of resistance

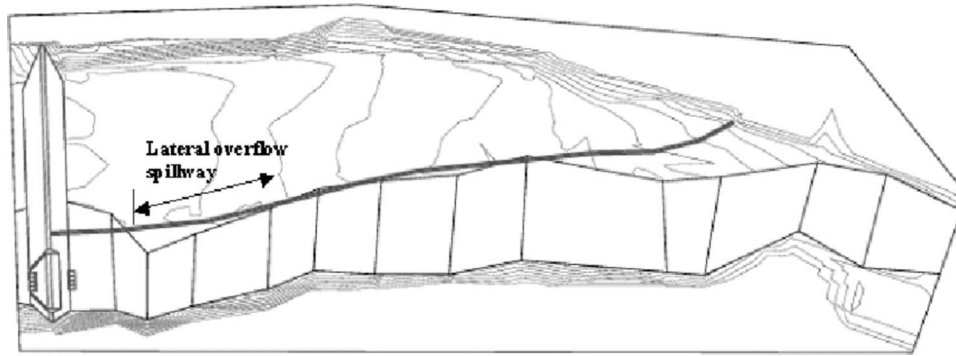


Fig. 3. Plan view of the VARA1 floodwater reservoir showing the dam and the longitudinal embankment along the right hydrographic bank with the lateral overflow spillway

must be smaller in the model. Thus, a thin layer of sand with an appropriate grain size has been glued on top of the modeled main channel in order to reproduce the correct prototype coefficient of resistance. Moreover, a long narrow area next to the river reach is sparsely wooded in the prototype, visible also from the aerial photograph of Fig. 1. The effect of the latter has been accounted for by reproducing an equivalent flow resistance for the case of vegetated channels, evaluated following Righetti et al. (2004). We have then obtained a corresponding value for the Chézy coefficient C and a resulting diameter of sand able to produce the required resistance.

The physical model was equipped with a hydraulic system able to reproduce the required time-dependent discharges. Flow control was obtained through a butterfly valve connected to a modulating actuator, which could be remote controlled. Finally, we have performed the following measurements: the model flow rate was measured using an orifice-plate flow meter with a pressure gauge; free surface elevation was measured using ultrasonic probes. The measurements have been synchronized through a data acquisition system in order to correlate the free surface level with the flowing discharge for the entire run. All the signals were simultaneously sampled, digitized with a 16-bit converter and continuously recorded on a computer. Signal prefiltering was provided in order to prevent measurement and digitalization errors.

Numerical Model

Governing Equations

Based on the assumption of hydrostatic pressure distribution and incompressible flows, the Saint-Venant equations for one-dimensional (1D) unsteady open-channel flow can be written as

$$\partial_t \mathbf{U} + \partial_x \mathbf{F} = \mathbf{S} \quad (2)$$

in which the vectors of unknowns \mathbf{U} , of fluxes \mathbf{F} , and of source terms \mathbf{S} , are given by

$$\mathbf{U} = \begin{bmatrix} A \\ Q \end{bmatrix}, \quad \mathbf{F} = \begin{bmatrix} Q \\ \Sigma \end{bmatrix}, \quad \mathbf{S} = \begin{bmatrix} q_l \\ gI_2 + gA(S_0 - S_f) + u_l q_l \end{bmatrix} \quad (3)$$

where $\Sigma = (Q^2/A) + gI_1$; t = time; x = longitudinal distance along a channel; A = wetted cross-sectional area; Q = water discharge; g = gravitational acceleration; I_1 = hydrostatic pressure force; S_0 = bed slope; S_f = friction slope; I_2 = side reaction term for nonprismatic channel; q_l = discharge per unit width due to lateral inflow/outflow; while u_l = velocity component of the lateral stream along the x -direction. The friction slope S_f of the channel can be expressed as

$$S_f = \frac{Q^2}{g(A^2 C^2 R)} \quad (4)$$

where R = hydraulic radius; and C = Chézy coefficient. Due to the complexity of natural geometry, the quantities A , $(A^2 C^2 R)$, are computed evaluating the integrals over the flow width using the Engelund approach (Engelund 1964):

$$A = \int_b [h - z_b(y)] dy \quad (5)$$

$$A^2 C^2 R = \left\{ \int_b c(y) [h - z_b(y)]^{3/2} dy \right\}^2 \quad (6)$$

where h = water surface elevation; b = flow width; $z_b(y)$ = bed elevation; and $c(y)$ the local Chézy coefficient.

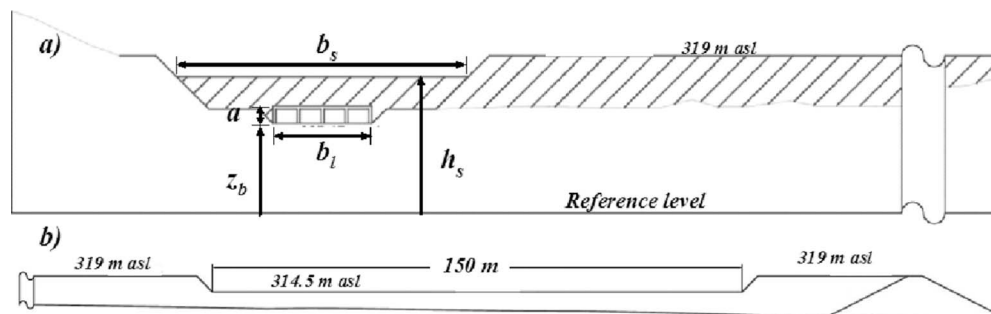


Fig. 4. Sketch of the main characteristics of the impounding structures: (a) dam; (b) lateral embankment

Table 1. Main Geometrical Characteristics of the Dams

	z_b [m AMSL]	a [m]	b_l [m]	b_s [m]	h_s [m AMSL]
VARA1	307.5	2.8	16	60	315
VARA2	267.6	3	24	150	277.6

Due to its hyperbolic nature, the system of governing Eq. (3) can be cast in characteristic form. If we neglect the source terms in the governing equations, we obtain the following compatibility equations

$$\frac{dQ}{dt} - c_{sw}(F \mp 1) \frac{dA}{dt} = 0 \quad (7)$$

to be integrated along characteristic paths defined by

$$\frac{dx}{dt} = \frac{Q}{A} \pm c_{sw} = c_{sw}(F \mp 1) \quad (8)$$

where $c_{sw} = Q/A \pm \sqrt{gA/b}$ = celerity of small amplitude waves; b = width of the water surface; and $F = Q/A\sqrt{gA/b}$ = Froude number. Alternatively, using the chain rule, compatibility Eq. (7) can be written in terms of variables Σ and Q as

$$\frac{d\Sigma}{dt} - c_{sw}(F \mp 1) \frac{dQ}{dt} = 0 \quad (9)$$

Numerical Solution

System of Eq. (3) is numerically integrated using a finite volume version of the predictor-corrector scheme of MacCormack (1971), which is second-order accurate and still widely used for solving open-channel flow problems. The solution at new time level $n+1$ at computational node i is obtained as follows

$$\mathbf{U}_i^{n+1} = \mathbf{U}_i^n - \frac{\Delta t}{\Delta x} [\mathbf{F}_{i+1/2}^n - \mathbf{F}_{i-1/2}^n] + \Delta t \mathbf{S}_i \quad (10)$$

where Δt and Δx = time and spatial steps used for integration. The intermediate flux computed at the intercell boundary $i+1/2$ is given by

$$\mathbf{F}_{i+1/2}^n = \frac{1}{2}(\mathbf{F}_{i+1}^n + \mathbf{F}_i^n) + \mathbf{D}_{i+1/2} \quad (11)$$

where

$$\mathbf{F}_i^n = \mathbf{F}(\mathbf{U}_i^n) \quad \mathbf{F}_i^n = \mathbf{F}(\mathbf{U}_i^n) \quad \mathbf{S}_i = \mathbf{S} \left[\frac{1}{2}(\mathbf{U}_i^n + \mathbf{U}_i^n) \right] \quad (12)$$

with

$$\mathbf{U}_i^n = \mathbf{U}_i^n - \frac{\Delta t}{\Delta x} (\mathbf{F}_{i+1}^n - \mathbf{F}_i^n) + \Delta t \mathbf{S}(\mathbf{U}_i^n) \quad (13)$$

The term $\mathbf{D}_{i+1/2}$ furnishes the scheme with total variation diminishing (TVD) dissipation capable of making the solution oscillation free while retaining second-order accuracy both in space and time. This is a very important property indeed when dealing with supercritical and rapidly varying flows with hydraulic jumps and bores. Details on the TVD corrections term, can be found in Garcia-Navarro and Alcrudo (1992) and Tseng (2003). The stability of the method is assured by imposing the Courant condition for computing the time step.

Boundary Conditions

If the computational domain is divided in M volumes, the finite-volume version of the MacCormack method [Eq. (10)] can be applied directly to all cells i , for $i=2, \dots, M-1$. For the first and M -th volume, which are adjacent to the upstream and downstream boundaries respectively, we only have one intercell flux. In order to find the solution at time level $n+1$ using Eq. (10), we have to find the upstream flux terms $F_{1/2}$ and their downstream counterparts $F_{M+1/2}$. Thus, for the Saint-Venant equations, the unknowns are $Q_{1/2}$, $\Sigma_{1/2}$, and $Q_{M+1/2}$ and $\Sigma_{M+1/2}$. In what follows we describe the procedure for the downstream boundary condition; the upstream boundary condition is treated similarly. Two different flow regimes are possible: subcritical flow ($F < 1$) or supercritical flow ($F > 1$). For $F < 1$, one exterior condition must be supplied, i.e., a prescribed rating curve that imposes a nonlinear relationship of the kind

$$Q_{M+1/2}^{n+1/2} = f(\Sigma_{M+1/2}^{n+1/2}, t^{n+1/2}) \quad (14)$$

Eq. (14) must be combined with a characteristic equation which takes information from the interior of the domain and projects it outside at the boundary. As in Capart et al. (1999), we assume the following approximation for the characteristic equation

$$(\Sigma_{M+1/2}^{n+1/2} - \Sigma_M^n) - c_{sw}(F - 1)(Q_{M+1/2}^{n+1/2} - Q_M^n) = 0 \quad (15)$$

Finally, the solution is obtained iteratively solving the two Eqs. (14) and (15). For supercritical flows, no exterior conditions are required, all the information necessary to obtain numerical fluxes $Q_{M+1/2}$ and $\Sigma_{M+1/2}$ come from the interior domain solving both Eqs. (9) discretized as in Eq. (15).

Modeling Description of Configurations M1 and L1

The numerical description of the two designed configurations $M1$ and $L1$ was implemented using the 1D model described in the previous section. During the rising limb of the flood wave, due to the presence of the dam, the water surface level increases. Once the top of the embankment height is reached, the floodplain starts to be inundated. The flooding mechanism has been modeled assuming that the rising (falling) velocity of the water level in the main channel $(dh_m)/(dt) = v_m$, could be different from the one of the floodplain $[(dh_f)/(dt) = v_f]$. Configuration $L1$ has been simulated imposing $v_m = v_f$ while configuration $M1$ has been modeled assuming that v_m differs from v_f . In particular, we have assumed that the floodplain starts to be inundated only after the water overflows the crest of the levee, which divides the main channel from the floodplain. The floodplain is assumed to behave as a reservoir of known geometry that is statically filled. The relationship between the volume and the water surface level inside the reservoir has been estimated from the topographic data and tested experimentally.

Initially, when the storage area is empty, the behavior of the lateral weir can be described by a broad-crested weir model, in which the overflow discharge $(q_{l(f)})$ depends exclusively on the water surface level in the main channel (free overflow). When the water level in the floodplain achieves the weir crest elevation, the two levels h_m and h_f begin to interact ultimately decreasing the overflow discharge $[q_{l(s)}]$: i.e., the overflow is submerged. The discharge that fills the storage area decreases and can be determined from the overflow depth, measured from the crest elevation (Y_0) and from the tailwater depth (Y_t), measured positively upwards from the weir crest (see Fig. 5). During the falling limb of the flood wave, direction of flow reverts, moving water from the

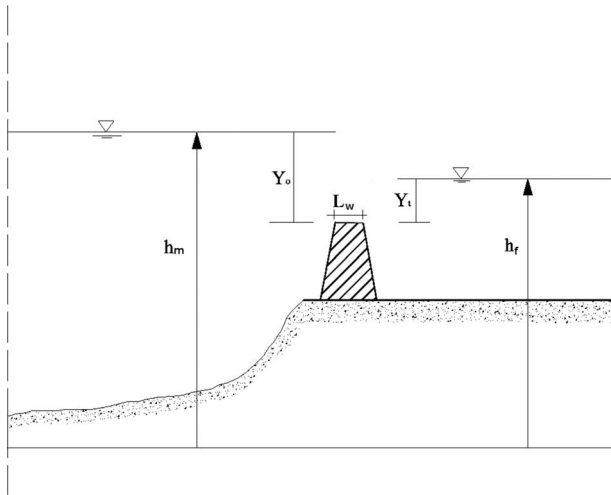


Fig. 5. Schematization for the submerged flow case

storage area to the main channel. When the water surface level in the storage area reaches the weir crest, the overflow ends.

The spillway law governing the lateral discharge has been defined as follows:

- Free overflow

The lateral discharge per unit width $q_{l(f)}$ is given by

$$q_{l(f)} = C_d(2gY_0^3)^{1/2} \quad (16)$$

where the discharge coefficient C_d was chosen as 0.385.

- Submerged overflow

For submerged overflow, $q_{l(s)}$ is obtained by reducing the lateral discharge $q_{l(f)}$. The relationship between $q_{l(s)}$ and $q_{l(f)}$ is given by

$$q_{l(s)} = \psi q_{l(f)} \quad (17)$$

where the reduction coefficient ψ depends exclusively on the submergence ratio S_r , which reads

$$S_r = \frac{Y_t}{Y_0} \quad (18)$$

The reduction factor ψ is evaluated by a power law of the form

$$\psi = (1 - P)^{1/n} \quad P = \frac{S_r - y_L}{1 - y_L} \quad 0 \leq P \leq 1 \quad (19)$$

with

$$y_L = 0.85 - 0.50\xi \quad (20)$$

and where $\xi = \frac{Y_0}{Y_0 + L_w}$ and L_w = crest length. The coefficient n has been chosen equal to 3 as suggested by Fritz and Hager (1998).

Results

Steady Flow Experiments

A first set of experiments was devoted to evaluate the rating curve appropriate for the kind of dam analyzed in the present study. The physical model was fed with different values of constant discharge Q (ranging between 44 and 822 m³/s), until steady flow conditions were achieved, and the level of the free surface upstream of the dam was measured and related to the Q value. Measurements were interpreted in terms of analytical rating curve

able to describe the different flow regimes depending on the inflow discharges and the level upstream the dam. All power laws can be easily obtained imposing the conservation of the total head, assuming the value of the velocity head negligible, which is in general true as shown in Savage and Johnson (2001). The resulting laws have an exponent equal to 3/2 when the flow crosses the critical depth, whereas the exponent 1/2 is derived when the behavior is similar to a sluice gate. Moreover, downstream submergence is not considered in the present analysis.

The analytical rating curve can be finally written as

- Regime A

$$Q = C_{Ql}\sqrt{2g}b_l(h - z_b)^{3/2} \quad (z_b < h < z_b + a) \quad (21)$$

where b_l = net width of the gate; C_{Ql} = discharge coefficient to be determined; and a = height of the bottom gate.

- Regime B

$$Q = C_{Ql}ab_l\sqrt{2g}(h - z_b)^{1/2} \quad (z_b + a < h < h_s) \quad (22)$$

- Regime C

$$Q = C_{Ql}ab_l\sqrt{2g}(h - z_b)^{1/2} + \phi(h)C_{Qs}b_s\sqrt{2g}(h - h_s)^{3/2} \quad (h_s < h < h_s + \delta) \quad (23)$$

where b_s = width of the spillway; $\phi(h)$ = function specified in the following in order to join Regime B smoothly with Regime D; while δ = smoothing function coefficient which is set, to 0.5 m.

- Regime D

$$Q = C_{Ql}ab_l\sqrt{2g}(h - z_b)^{1/2} + C_{Qs}b_s\sqrt{2g}(h - h_s)^{3/2} \quad (h > h_s + \delta) \quad (24)$$

The coefficients C_{Ql} and C_{Qs} , obtained by means of a nonlinear regression on the experimental measurements, were found as

$$C_{Ql} = 0.588 \quad C_{Qs} = 0.354 \quad (25)$$

The function $\phi(h)$ was introduced in the intermediate Regime C in order to obtain a continuous transition from the half-power law of the Regime B to the 3/2 law of the Regime D. A possible structure for the function ϕ that fulfills the above requirements may be written as

$$\phi(h) = \frac{\arctan[(h - h_s - \delta)20]}{\pi} + \delta \quad (26)$$

The comparison between the experimental measurements and the analytical interpretation given above, shown in Fig. 6, demonstrates good agreement in all the regimes of the rating curve.

A series of steady flow experiments varying the original geometry of the bottom gate, reducing the width by half, was also performed. The analytical rating curve, keeping the coefficients C_{Ql} and C_{Qs} equal to the values reported in Eq. (25), is still in good agreement with experimental observation as shown in Fig. 6. The latter result suggest that the rating curve described by Eqs. (21)–(24) may be extended to any composite transversal structure with a design similar to the one here investigated (bottom gate and overflow spillway) changing only the geometrical dimensions.

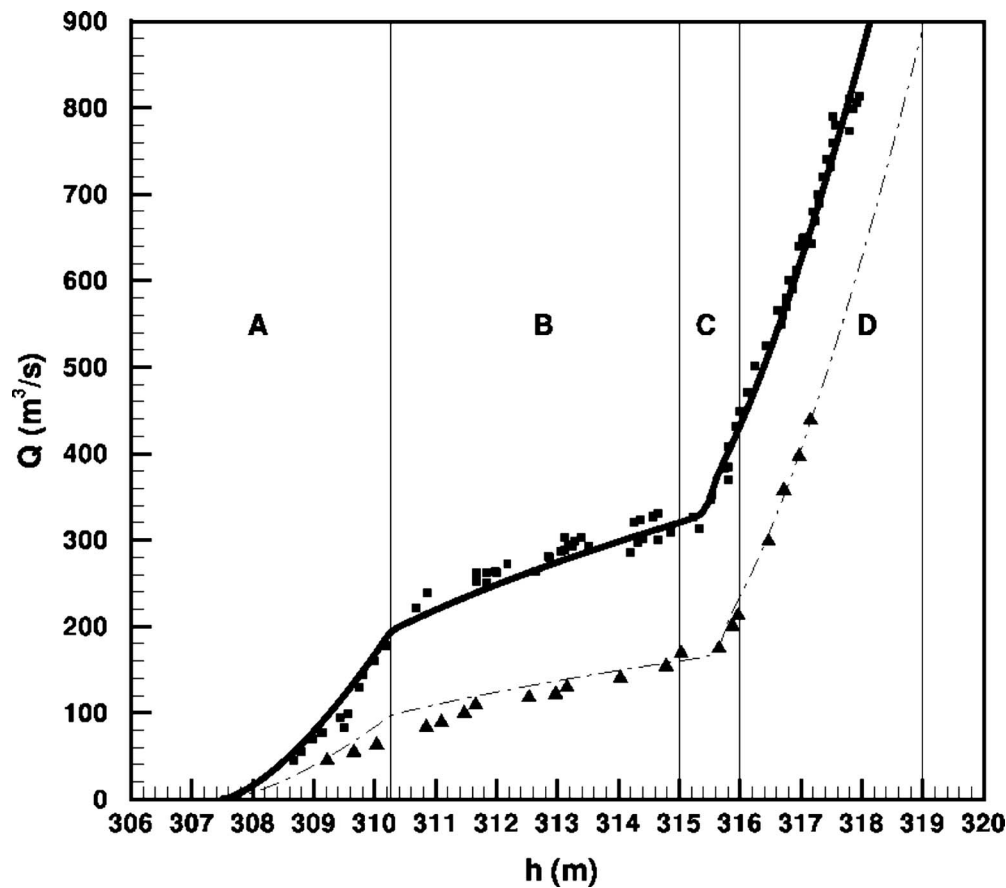


Fig. 6. Comparison between the measured rating curve (symbols) and the analytical rating curve given in Eqs. (21)–(24) for the designed geometry (solid line) and the modified geometry (dashed line). The capital letters correspond to the different regimes.

Unsteady Flow Experiments: Numerical versus Experimental Results

In this section, the results obtained numerically with the flood propagation model have been compared against the experimental measurements. The numerical simulations of the VARA1 were performed imposing at the inlet section hydrographs with different return period and, at the outlet section, the empirical rating curve [Eqs. (21)–(24)] representing the dam; 140 equal spaced cells with $\Delta x=7$ m has been used. For the sake of brevity only results obtained with the 30-year return period events will be presented. Initially, for small discharge values, the flow is characterized by supercritical conditions. During the rising limb of the flood, the downstream water level rises imposing locally a subcritical flow. Upstream and downstream flows are joined by a hydraulic jump that amplifies during its upstream migration. During the falling limb of the flood this process reverts and the hydraulic jump travels in the downstream direction.

Configuration L1

In Fig. 7, a comparison between the inflow ($T_r=30$ years) and outflow hydrographs for the L1 configuration is shown. The agreement between numerical and experimental results is fairly good everywhere but in proximity of the peak of the hydrograph. In fact, the numerical model predicts a water surface level above the broad crest of the top of the spillway, with an abrupt growth of the outflow discharge, whereas during the experiments the water level remains below of the top of the spillway. This discrepancy, which appears large in terms of discharge, is more ac-

ceptable if the water level is considered (see Fig. 8). In fact, the maximum difference between the water surface level experimentally measured and numerically computed is 85 cm over a water depth of 8 m, corresponding to a relative error of 10%. This small error on the prediction of the water level results in a larger error in the discharge since the water surface level is very close to the broad crest level (315 m AMSL), where the slope of the rating curve changes rapidly. This error is most likely due to 2D effects, that are not taken into account by the 1D numerical model. In fact, the presence of the floodplain on the right side of the river reach generates a large scale horizontal recirculation, observed during the experimental runs, which can delay the propagation of the flood wave.

Configuration M1

The results obtained for the M1 configuration are shown in Figs. 9 and 10. Agreement between the results obtained from numerical simulations and experiments is fairly good, due to the fact that the longitudinal embankment constrains the river reach to behave as a confined channel, thus with a hydraulic behavior that can be appropriately described even with a 1D model. In this case, the agreement between the numerical prediction and the experimental measurements is satisfactory even near the peak of the hydrograph. The water discharge predicted during the falling limb of the hydrograph exceeds that measured in the physical model. This is due to the fact that the emptying process of the storage area, which take places once the peaks pass through, is not simulated numerically, whereas in the physical model it is.

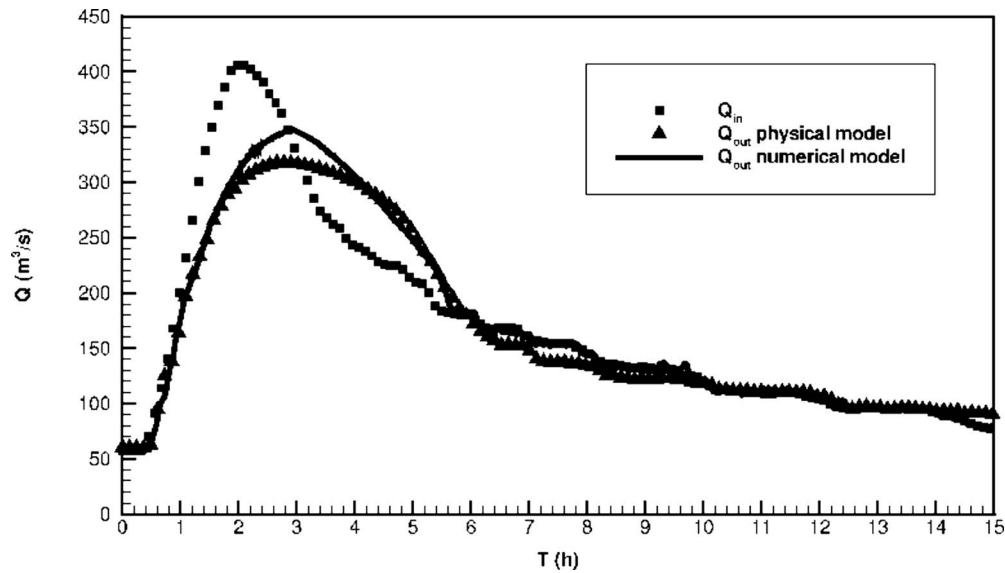


Fig. 7. L1 comparison between the inflow and outflow hydrographs: $T_r=30$ years

Flood Attenuation Efficiency

The comparison between the efficiency computed for both configurations L1 and M1, plotted as a function of the inflow discharge peak, is shown in Fig. 11. For the L1 configuration the following considerations stand out. The maximum efficiency (20%) is achieved for the design discharge Q_d (416 m³/s) having a 30 years return period. Efficiency decreases for discharges which are either higher or lower than the designed discharge, and tends to vanish as the discharge increases approaching the 200-year discharge ($Q=815$ m³/s). This reflects the choice adopted for designing the attenuation flood works of the river reach under consideration. The efficiency is even significant (greater than 5%) for discharge values having a return period greater than 100 years. The agreement between the numerical results and the experimental observations is, in this case, less satisfactory. A difference of 5% in the evaluation of the outflow discharge becomes a difference of 45% in terms of efficiency. The predicted water depth has

a maximum difference with the observed values of 16% and a mean error less than 2%. Finally, the maximum of the numerically computed efficiency is obtained for a discharge value that is slightly smaller than what is experimentally observed. For the M1 configuration the behavior of the flood mitigation is qualitatively analogous to the L1 case, with a better quantitative description. This confirms that the hydrodynamics of the storage area is better described in this configuration, with a consequent more detailed prediction of the flood reduction effect. The comparison between the two efficiencies evaluated for the two configurations, L1 and M1, suggests some conclusions. The maximum efficiency in the M1 case is slightly better than the L1 case with, however, a defense structure that has a more significant environmental impact. For discharge values having a return period less than 30 years, the efficiency of the L1 configuration is systematically greater than the efficiency for the M1 configuration. This is expected, since the M1 configuration has an embankment that confines the flow in

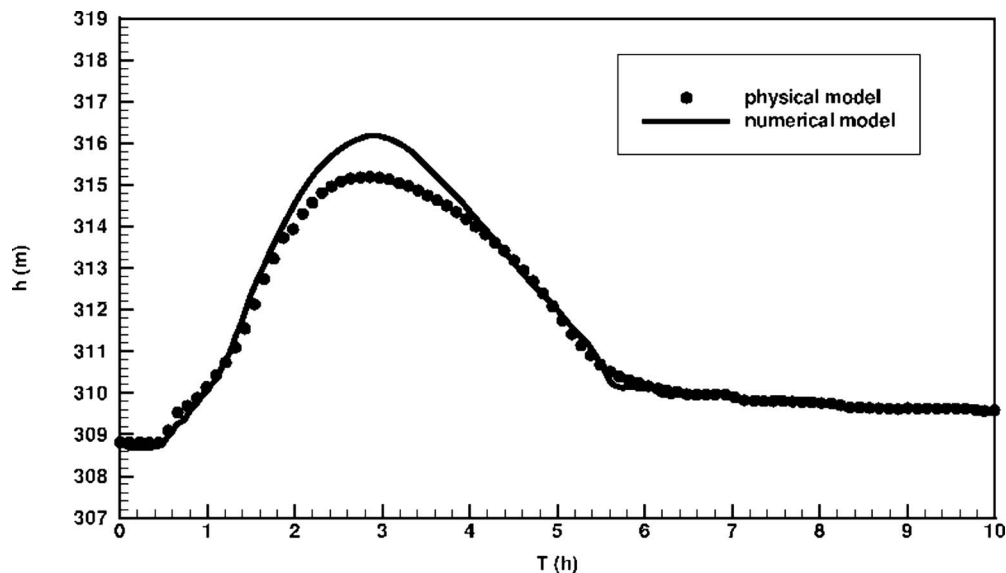


Fig. 8. L1 water surface level just upstream the dam: $T_r=30$ years

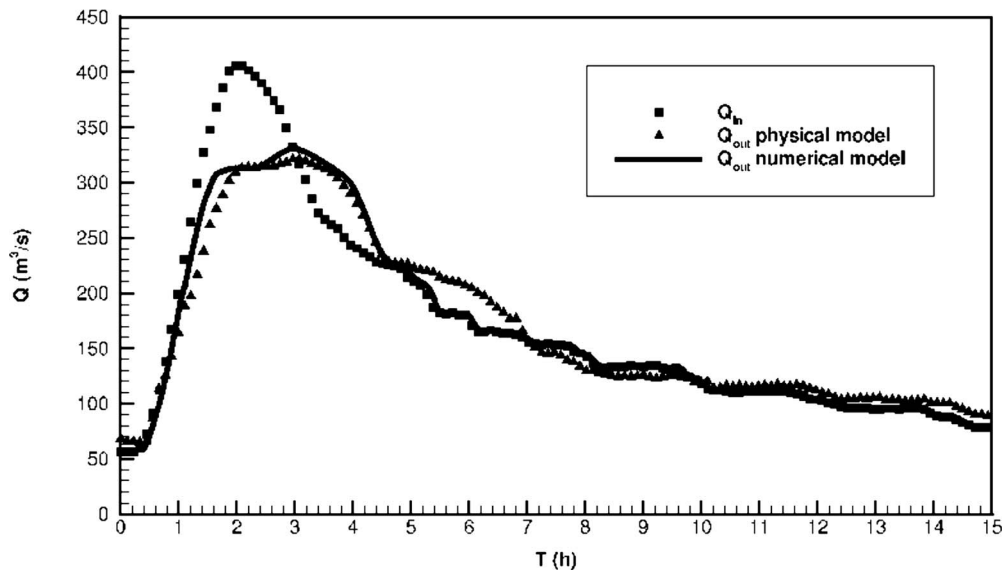


Fig. 9. M1 comparison between the inflow and outflow hydrographs: $T_r=30$ years

the main channel until the water depth reaches the crest of the lateral spillway and part of the discharge inundates the floodplain, producing an attenuation of the flood itself. However, differences tends to disappear for discharge with a return period greater than 30 years and, for both the configurations, the flood attenuation efficiency rapidly decreases. In fact, for such hydrological events the available flood storage volume is already occupied long before the peaks passes, strongly reducing the efficiency.

Flood Attenuation Efficiency of the System

Since in the Magra and Vara basins the construction of a series of floodwater storages for flood prevention is planned, an obvious question to be answered in this case is what would be the efficiency of the entire system and how the latter is related to the

efficiency of the single floodwater storage. In the present study, this analysis was possible only via numerical simulations, since the physical model simulated only one of the two floodwater defense systems. Because we have demonstrated that the numerical model is able to reproduce correctly the results for a single structure, as shown in the previous sections, a series of numerical simulations was conducted in order to predict the flood attenuation efficiency for the entire system (VARA1 plus VARA2). In this case, the discharge flowing into the VARA2 flood water storage area is affected by the attenuation effect produced by the upstream one. Indeed, the output discharge from VARA1 is the input for the downstream flood water storage. Furthermore, four minor tributaries join the Vara River along its reach between the VARA1 and VARA2. The discharge flowing into the main chan-

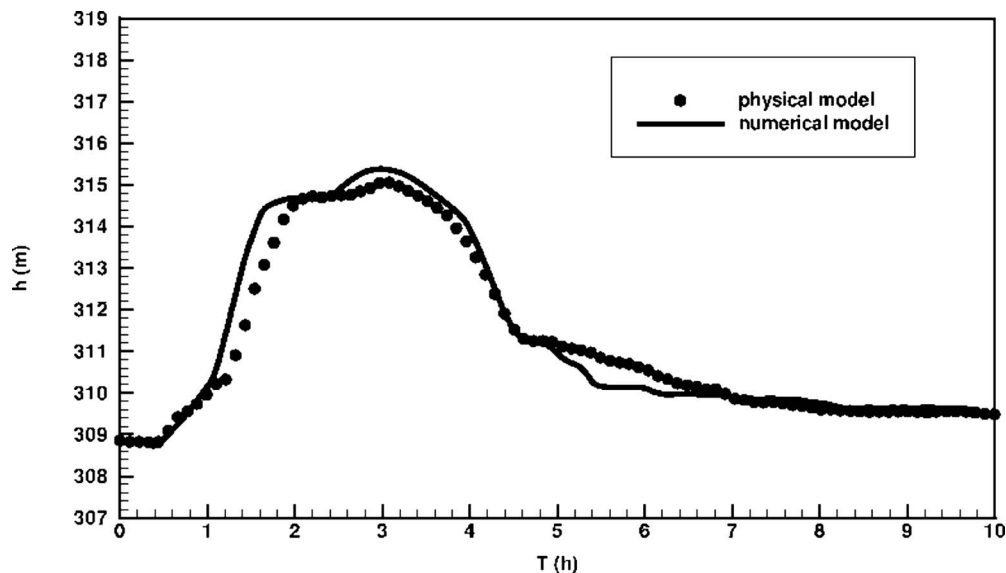


Fig. 10. M1 water surface level upstream the dam: $T_r=30$ years

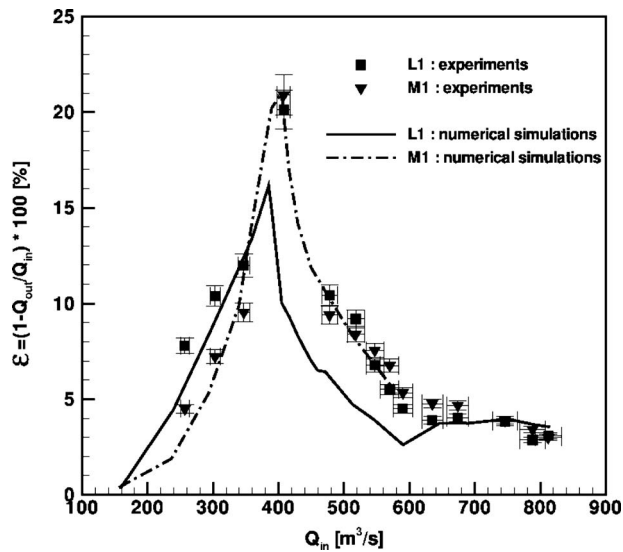


Fig. 11. Flood attenuation efficiency: numerical results superimposed to the experimental results for both configurations, i.e., M1 and L1

nel must be accounted for and summed to the output discharge from the VARA1. The resulting flood attenuation efficiency curve as a function of the flow discharge is shown in Fig. 12. As for the VARA1 the best efficiency is recovered for the design discharge, corresponding to a return period equal to 30 years. Moreover, the shape of the efficiency curve is similar to the one obtained for the VARA1 case, consistently with the analog geometrical configuration. Also in this case, discharges far from the design value produces a substantial decrease in the flood attenuation efficiency.

If we now consider the flood mitigation obtained by the simultaneous presence of the two detention systems, the highest attenuation is again recovered for the design discharge, where the two systems show their efficiency peak, and its value is equal to 20.0%.

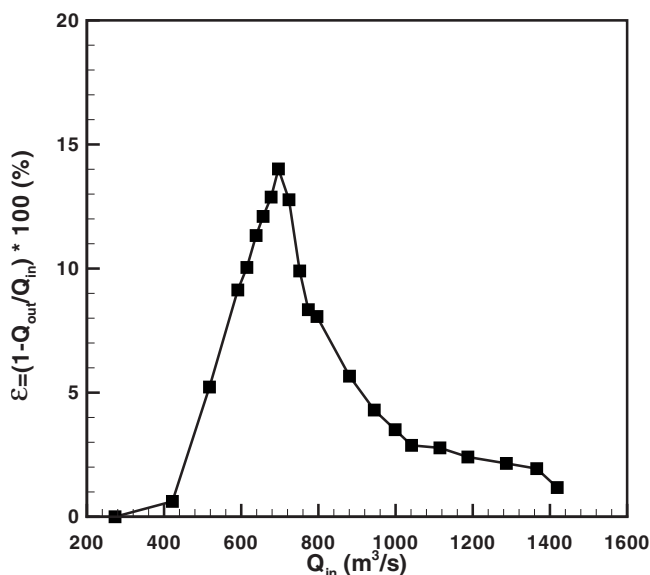


Fig. 12. Flood attenuation efficiency for the VARA2 floodwater storage

The above result can be generalized to a system of detention reservoirs, including the contribution to the main channel discharge due to the presence of tributaries. In fact, the flood attenuation efficiency of a system composed by N basins can be expressed by the following relationship:

$$\varepsilon_{1,N} = 1 - \frac{\prod_{i=1}^N (1 - \varepsilon_i) + \sum_{i=1}^N \frac{Q_T^{i-1}}{Q_{IN}^1} \prod_{k=i}^N (1 - \varepsilon_k)}{1 + \frac{1}{Q_{IN}^1} \sum_{i=2}^N Q_T^{i-1}} \quad (27)$$

where ε_i =attenuation produced by the i -th basin; Q_T^i =total tributary discharge in the reach between the reservoir i and $i+1$; and Q_{IN}^1 =discharge at the most upstream river section. The above formulation is valid under the hypothesis that the flood attenuation is negligible during its propagation along the main channel. Eq. (27) in the absence of tributaries reduces to

$$\varepsilon_{1,N} = 1 - \prod_{i=1}^N (1 - \varepsilon_i) \quad (28)$$

Conclusions and Future Developments

The hydraulic design of a system of two flood control detention reservoirs has been investigated in detail through both experimental runs on a physical model and 1D numerical simulations. From the analysis of the results obtained for the specific case study presented some general conclusions can be drawn, which can be briefly summarized as follows:

- A rating curve able to describe a composite hydraulic behavior of a structures of the kind as the one designed for the present dam has been derived and tested experimentally; the proposed formulation eventually depends only on the geometrical characteristics of the dam itself (sluice gate and spillway);
- The 1D numerical model fit the experimental measurements, provided that correct boundary conditions are imposed; the agreement between the numerical predictions and the experimental observations is fairly good during the entire propagation of the flood;
- If correctly designed, a system of relatively small detention reservoirs distributed inside the watershed of the main river and its tributaries is able to produce a reasonable flood mitigation, such that their construction is justifiable; in this regard, it is fundamental to analyze a wide range of return periods in order to assess the response of the flood control measure to different hydrological scenarios; and
- A simple relationship for the flood attenuation efficiency has been proposed for a system of reservoirs, which might be used in order to estimate the response of the entire system based on the knowledge of the performance of the single flood control system.

Future investigations will regard the impact of flood defense measures as the ones studied on the natural balance of sediment and water quality. In particular, sediment deposition is likely to occur behind the dam [see the example given in (Siviglia et al. (2008))] producing a decrease, in the long run, of the storage capacity and an abrupt disconnection for the natural sediment conveyance. For the above reason, experimental and numerical tests including the sediment transport have been planned to be per-

formed on the physical model and using a morphological numerical model, with the aim of investigating all the aforementioned scenarios.

Acknowledgments

The present research project has been cofunded by Autorita' di Bacino del Fiume Magra. The MODITE project is also acknowledged.

Notation

The following symbols are used in this paper:

- A = cross-sectional area (m^2);
- a = sluice gate height (m);
- b = width of the water surface (m);
- b_l = net width of the bottom gate (m);
- b_s = width of the top spillway (m);
- C_d = discharge coefficient;
- C_{Ql} = discharge coefficient;
- C_{Qs} = discharge coefficient;
- $c(y), C$ = local and global conductivity coefficient;
- c_{sw} = celerity of small amplitude waves (m/s);
- \mathbf{D} = vector of TVD terms;
- \mathbf{F} = vector of fluxes;
- F = Froude number;
- g = acceleration due to gravity (m/s^2);
- h = water surface elevation (m);
- h_s = top spillway elevation (m);
- h_f = water surface elevation in the floodplain (m);
- h_m = water surface elevation in the main channel (m);
- I_1 = first moment of the wetted cross section (m^3);
- I_2 = spatial variation of the first moment (m^2);
- L_w = crest length (m);
- Q = discharge (m^3/s);
- Q_{IN} = peak of the hydrograph (m^3/s);
- Q_{IN}^1 = discharge at the most upstream river section;
- Q_{OUT} = maximum discharge that flows through the dam; (m^3/s);
- Q_T^i = total tributary discharge between the reservoir i and $i+1$ (m^3/s);
- q_l = lateral discharge (m^2/s);
- $q_{l(f)}$ = overflow discharge (m^2/s);
- $q_{l(s)}$ = overflow discharge reduction (m^2/s);
- \mathbf{S} = vector of source terms;
- S_f = friction term;
- S_r = submergence ratio;
- S_0 = longitudinal slope;
- \mathbf{U} = vector of conservative variable;
- u_l = velocity component of the lateral stream along the x -direction; (m/s);
- v_f = rising/falling velocity in the floodplain (m/s);
- v_m = rising/falling velocity in the main channel (m/s);

- Y = water depth (m);
- Y_r = tailwater depth (m);
- Y_0 = overflow depth, measured from the crest elevation (m);
- z_b = bed elevation;
- $\Delta x, \Delta t$ = spatial and time steps;
- δ = smoothing function coefficient;
- ϵ = flood attenuation efficiency;
- ϵ_i = attenuation produced by the i -th basin;
- $\epsilon_{1,N}$ = attenuation efficiency of a system composed by N basins;
- Ψ = reduction coefficient;
- Σ = flux of momentum equation; and
- Φ = rating curve function.

References

- Avakyan, A. B., and Polyushkin, A. (1989). "Flood control experience in the usa." *Power Tech. and Eng.*, 23(1), 53–58.
- Bunte, K., and Abt, S. R. (2001). "Sampling surface and subsurface particle-size distributions in wadable gravel- and cobble-bed streams for analyses in sediment transport, hydraulics, and streambed monitoring." *Gen. Tech. Rep. No. RMRS-GTR-74*, U.S. Dept. of Agriculture, Forest Service, Rocky Mountain Research Station, Fort Collins, Colo.
- Capart, H., Bogaerts, C., Kevers-Leclercq, J., and Zech, Y. (1999). "Robust numerical treatment of flow transitions at drainage pipe boundaries." *Water Sci. Technol.*, 39(9), 113–120.
- Engelund, F. (1964). "Book of abstracts." *Rep. No. 6*, Univ. of Denmark.
- Fritz, H. M., and Hager, W. H. (1998). "Hydraulics of embankment weirs." *J. Hydraul. Eng.*, 124(9), 963–971.
- Garcia-Navarro, P., and Alcrudo, F. (1992). "1D open channel flow simulation using TVD McCormack scheme." *J. Hydraul. Eng.*, 118(10), 1359–1373.
- Giesecke, J. (2007). "Dams and flood control-systems of detention reservoirs in southwestern Germany." *Proc., 14th German Dam Symp.*, (http://www.talsperrenkomitee.de/german_research/index.cgi/page/2).
- McCormack, R. (1971). "Numerical solution of the interaction of a shock wave with a laminar boundary layer." *Proc. 2nd Int. Conf. on Numerical Methods in Fluid Dynamics*, Springer, Berlin, 151–163.
- Parker, G. (1990). "Surface-based bedload transport relation for gravel rivers." *J. Hydraul. Res.*, 20(4), 417–436.
- Righetti, M., Armanini, A., and Rampanelli, L. (2004). "Effetto della scabrezza di parete in alvei vegetati." *Proc., 29th Convegno Nazionale di Idraulica e Costruzioni Idrauliche*, BIOS, 549–554.
- Savage, B. M., and Johnson, M. C. (2001). "Flow over ogee spillway: Physical and numerical model case study." *J. Hydraul. Eng.*, 127(8), 640–649.
- Siviglia, A., Nobile, G., and Colombini, M. (2008). "Quasi-conservative formulation of the one dimensional Saint Venant-Exner model." *J. Hydraul. Eng.*, 134(10), 1521–1526.
- Slutzman, J., and Smith, J. (2006). "Effects of flood control structures on flood response for hurricane Floyd in the Brandwyne Creek Watershed, Pennsylvania." *J. Hydrol. Eng.*, 11(5), 432–441.
- Tseng, M. (2003). "The improved surface gradient method for flow simulation in variable bed topography channel using tvd-mccormack scheme." *Int. J. Numer. Methods Fluids*, 43, 71–91.
- Wu, B., Wang, G., Ma, J., and Zhang, R. (2005). "Case study: River training and its effects on fluvial processes in the Lower Yellow River, China." *J. Hydraul. Eng.*, 131(2), 85–96.